J. exp. Biol. ***180***, *285-310 (1993)*
Printed in Great Britain © The Company of Biologists Limited 1993

GLIDING BIRDS: REDUCTION OF INDUCED DRAG BY WING TIP SLOTS BETWEEN THE PRIMARY FEATHERS

VANCE A. TUCKER

Department of Zoology, Duke University, Durham, NC 27706, USA

Accepted 5 March 1993

Summary

1. The feathers at the wing tips of most birds that soar over land separate both horizontally and vertically in flight to form slotted tips. The individual feathers in the slotted tips resemble the winglets used on the wing tips of some aircraft to reduce induced drag.

2. A wing that produces lift leaves a pair of vortex sheets in its wake. Wing theory shows that winglets can reduce the kinetic energy left in the vortex sheets, and hence the induced drag, by spreading vorticity both horizontally and vertically.

3. This paper describes the aerodynamic forces on a wing made of a base wing and different wing tips. The feathered wing tip was slotted and was made of four primary feathers from a Harris' hawk (*Parabuteo unicinctus*). The Clark Y tip was unslotted and was made of balsa wood shaped to a Clark Y aerofoil. The balsa feather tip was slotted and was made of three balsa wood wings shaped like feathers.

4. The base wing in a wind tunnel at an air speed of $12.6\,m\,s^{-1}$ generated upwash angles as high as 15° at the end of the wing when the angle of attack of the wing was 10.5°. The feathered tip responded to upwash by increasing its lift to drag ratio (*L*/*D*) by 107%, from 4.9 to 10.1, as the angle of attack of the base wing increased from 4° to 14°. The *L*/*D* values of the balsa feather tip and the Clark Y tip increased by 49% and 5%, respectively, for the same change in angle of attack.

5. With the angle of attack of the base wing fixed at 13°, changing the angle of attack of the wing tip changed the drag of the base wing. The drag of the base wing increased by 25% as the angle of attack of the Clark Y tip increased from 0° to 15°. The base wing drag decreased by 6% for the same change in the angle of attack of the feathered tip.

6. The total drag of the wing with the feathered tip was 12% less than that of a hypothetical wing with the same lift and span, but with tip feathers that did not respond to upwash at the end of the base wing. This value is consistent with wing theory predictions on drag reduction from winglets.

7. Wings with the tip and the base wing locked together had lift and drag that increased with increasing base wing angle of attack, as expected for conventional wings. Span factors were calculated from these data – a large span factor indicates that a wing has low induced drag for a given lift and wing span. The wing with the Clark Y

Key words: bird, effective aspect ratio, effective span, flight, flow visualization, free vortex, emarginated feathers, Harris' hawk, non-planar wings, *Parabuteo unicinctus*, profile drag, soaring, slotted tips, span factor, tip feathers, tip vortex, trailing vortex, vortex spreading, vortex diffusion, winglets.

tip had a span factor that decreased from 1 to 0.75 as the angle of attack of the base wing increased. Over the same range of angle of attack, the span factor of the wing with the feathered tip remained constant at 0.87. As the angle of attack of this wing increased, aerodynamic forces spread the feathers vertically to form slots. With fully formed slots, the wing had a higher span factor than the wing with the unslotted Clark Y tip.

8. Flow visualization with helium-filled bubbles showed that the addition of two winglets to the tip of a model wing spread vorticity both horizontally and vertically in the wake of the tip.

9. These observations taken together provide strong evidence that the tip slots of soaring birds reduce induced drag in the sense that the separated tip feathers act as winglets and increase the span factor of the wings.

Introduction

Birds that soar over land usually have wings with separated feathers at the tips. Seen from below, these feathers form prominent slots during gliding (Fig. 1). Seen from head on (Fig. 2), they bend upwards and spread out vertically. The tip feathers obviously produce lift, because they bend downwards when the bird is not flying. I shall use the term ‘slotted tips’ to refer to wing tips with these separated feathers.

Biologists have speculated for years about the functions, other than lift production, of slotted tips. The following have been suggested (see reviews by Graham, 1932; Withers, 1981; Kerlinger, 1989; Norberg, 1990; Spedding, 1992): reduction of sound, prevention of feather wear, reduction of wing twisting, control and stabilization of roll, prevention of stall, attainment of high lift coefficients and reduction of drag.

The individual feathers in slotted tips are thought to reduce drag by acting as winglets (Cone, 1964; Hummel, 1980; Kuethe and Chow, 1986; Spillman, 1987; Spedding, 1992). Winglets are small wings attached to the tips of a base wing. They reduce drag by spreading vorticity vertically in the wake of the wing and are used on aircraft wings (Lambert, 1990) and on the keels of sailboats (Kyle and Eggleston, 1992). This paper summarizes the theory of winglets and investigates experimentally whether the slotted tips of soaring birds act as winglets.

Conventions

Air velocity, the coordinate system and aerodynamic forces

An observer of a bird in natural flight regards a bird as moving through the air. This study regards the bird as stationary, with the air moving past it at velocity V relative to a three-dimensional, orthogonal coordinate system attached to the bird (Fig. 3). The x axis is parallel to V, the y axis is horizontal, and the z axis is perpendicular to the x,y plane.

A wing exposed to moving air generates an aerodynamic force (F) that makes an angle (γ) with the x axis (Fig. 3). This force has three components: lift (L) and drag (D), which are perpendicular and parallel, respectively, to the direction of V (Fig. 3), and a

lateral component that is parallel to the *y* axis. When the lateral component is negligible,

$$L = F\sin\gamma, \quad (1)$$

$$D = F\cos\gamma, \quad (2)$$

and the ratio of lift to drag is:

$$L/D = \tan\gamma. \quad (3)$$

Wing nomenclature

Aerodynamic terminology uses the singular ‘wing’ to refer to a wing of full- or semi-span. I use the singular form when discussing aerodynamics and the plural ‘wings’ when discussing the full-span wing of a bird.

The wing span is the maximum distance between the wing tips, measured parallel to the *y* axis. The wing chord is the distance between the leading and the trailing edges of the

Fig. 1. Slots formed by the separated primary feathers at the wing tips. California condor (*Gymnogyps californianus*), maximum wing span, 3m. Photograph courtesy of Noel Snyder, Portal, Arizona.

wing, measured in the *x*,*z* plane. The aerofoil is the periphery of the wing in a cross section parallel to the *x*,*z* plane. The root of a wing is the region that connects to the fuselage of an aircraft or the shoulder region of a bird.

This paper uses special terms to describe a model wing. The model wing is a semi-span that has two parts: a base wing and a wing tip mounted at the end of the base wing. The term ‘base wing’ refers to any wing exclusive of its tips. The wing tip and the end of the base wing are different structures, and the terms ‘tip’ and ‘end’ distinguish between them.

The angle of attack of the base wing or wing tip is measured in a plane parallel to the *x*,*z* plane and is the angle between the *x* axis and a reference line. The Materials and methods section describes the reference lines for the model base wing and different wing tips.

Theory and experimental approach

This section briefly summarizes the aerodynamic concepts that underlie the experiments in this study. I use conventional aerodynamic terminology but omit formal definitions (see von Mises, 1959; Kuethe and Chow, 1986; Katz and Plotkin, 1991).

Induced drag

Drag and energy loss in the wake

A wing of finite span that produces lift leaves circulating air and kinetic energy in its wake. In an ideal fluid (which has no viscosity), this energy accounts for the drag of the wing, since it is left behind at a rate that is the product of drag and V (Durand, 1943, pp. 125–128). Wing theory calculates the lift and drag on the wing, assuming air to be an ideal fluid. The drag arises solely from lift production and is usually called induced drag to distinguish it from profile drag (discussed in a later section), which arises in a viscous fluid. I refer to induced drag simply as ‘drag’ when discussing wing theory.

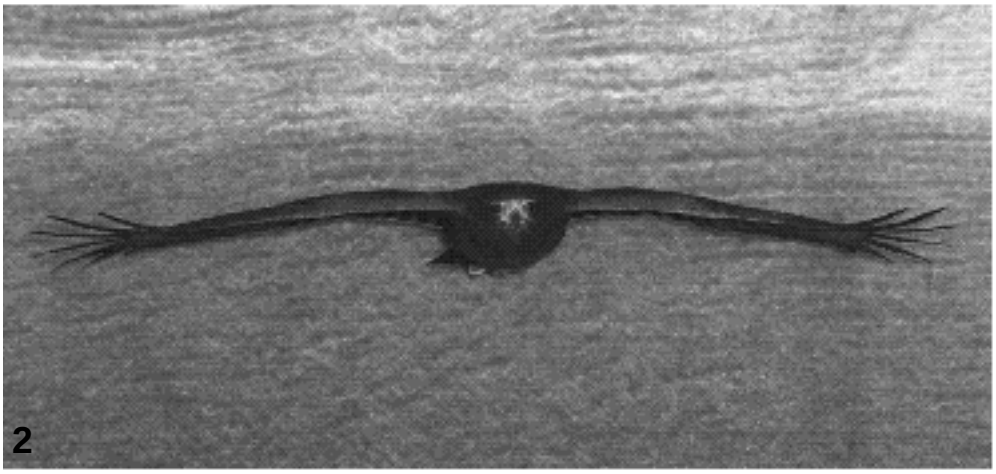

Fig. 2. Vertical separation between the feathers in the slotted wing tips. The Harris’ hawk (*Parabuteo unicinctus*) is gliding at 8.0 m s^{-1} with a wing span of 0.92m in a wind tunnel. Air flows over the bird and through the porous fibreglass matting in the background.

Wing theory attributes the circulation in the wake to two free vortex sheets, one behind each semi-span of the wing. The lift of the wing determines the circulation around each vortex sheet but not the kinetic energy in the wake. The kinetic energy, and hence the drag, depends both on the circulation and on how the the vortex sheet is spread out in space. A wing that spreads out the vortex sheet can decrease the drag for a given amount of lift.

Vortex spreading by two types of wings is of interest in this paper. Planar wings have a trailing edge that is a straight line between the wing tips. Non-planar wings have a trailing edge that is a curved line in a plane parallel to the *y*,*z* plane – i.e. the wing bends upwards or downwards between root and tip. A planar wing spreads vorticity only horizontally along the trailing edge, but a non-planar wing can spread vorticity both horizontally and vertically.

Wing theory shows that vorticity spreading by a planar wing depends on the lift distribution – the lift per unit span at each point on the wing between the root and the tip. Drag is minimal for a given lift and span when the lift distribution is elliptical, with the lift per unit span changing from a maximum at the root to zero at the tip. The minimum drag ($D_{i,min}$) is:

$$D_{i,min} = L^2/(\pi q b^2), \tag{4}$$

where L is lift, b is wing span and q is the dynamic pressure:

$$q = \rho V^2/2, \tag{5}$$

where ρ is the density of air.

Planar wings that have non-elliptical lift distributions have greater drag values, and the induced drag factor (k) accounts for the increase:

$$D_i = kL^2/(\pi q b^2). \tag{6}$$

The value of k is unity for a planar wing with an elliptical lift distribution but greater than 1 for other lift distributions. (The reciprocal of k is often used in the aerodynamic literature.)

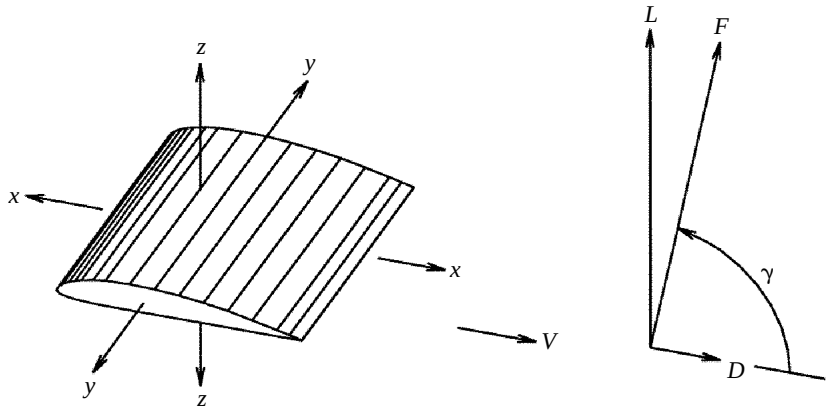

Fig. 3. Coordinate system and aerodynamic force components defined relative to air moving past a wing at free-stream velocity V. The aerodynamic force (F) on the wing is inclined at angle γ to V. The x axis and the drag component (D) of force are parallel to V. The z axis and the lift component (L) of the force are perpendicular to V. The y axis is horizontal.

A non-planar wing may have k values less than 1 because it spreads vorticity both horizontally and vertically. For example, k is 0.5 for a circular, ring-shaped wing (Cone, 1962). Vertically separated winglets at the tip of a planar wing reduce k because they make the wing non-planar and spread vorticity vertically (Munk, 1921; Mangler, 1938; Cone, 1962; Whitcomb, 1976; Flechner *et al.* 1976; Asai, 1985). Horizontal winglets, in tandem one behind another, form slots, but do not make the wing non-planar and do not reduce k (Munk, 1921; Hummel, 1980).

All soaring birds with slotted tips display vertical separation between the tip feathers in flight (Fig. 2), suggesting that these feathers reduce drag by acting as winglets. The significance of vertical separation has sometimes been overlooked. Newman's (1958) statement that tip slots do not reduce induced drag applies only to feathers in tandem. Oehme (1977) calculated a drag reduction from tip feathers in tandem but did not fully account for the interaction between the free vortices from the feathers.

Drag and local flow near the wing

The free vortices in the wake of the wing cause the flow near the wing (the local flow) to have a downward velocity component (downwash) between the wing tips. Downwash causes the drag on the wing (for example, see Jones, 1950, and Fig. 4 in this paper).

Local flow with an upward component (upwash) may reduce drag or even generate thrust (Fig. 4). Flapping wings and propellors produce thrust by this means. Spillman (1987) describes how winglets (which he calls wing tip sails) can have reduced drag because they extend into upward local flow at the ends of a wing that produces lift. This local flow arises because the pressure beneath the wing is greater that that above, and air flows upwards around the end of the wing.

Profile drag

A real wing has greater drag than predicted by wing theory because of the viscosity of air. The total drag (D) of the wing is the sum of this additional drag (profile drag, D_{pr}) and induced drag (D_i):

$$D = D_{pr} + D_i. \tag{7}$$

One can directly measure the total drag of a wing a wind tunnel but not the profile drag or the induced drag. Usually, either the induced or profile drag is calculated from theory or set to zero by experimental conditions, and subtracted from total drag to find the remaining drag term in equation 7. Profile drag is sometimes determined indirectly by measuring q in the wake of the wing (Betz, 1925; Pennycuick *et al.* 1992).

von Mises (1959, p. 142) describes a model (I shall call it the partition model) that partitions the total drag of a wing into profile drag and induced drag. The partition model describes how the lift and total drag of a wing vary with angle of attack at constant speed, and it yields a constant value for profile drag as the angle of attack of the wing changes. The partition model is reasonably accurate for real wings with a range of angles of attack over which the lift increases linearly.

I used the following form of the partition model to separate induced and profile drag in this study. The total drag of the wing is the sum of profile and induced drag (from equations 6 and 7):

$$D = D_{pr,0} + kL^2/(\pi q b^2), \tag{8}$$

where profile drag has the constant value $D_{pr,0}$. Both lift (L) and total drag (D) of a wing can be measured. If D is plotted against L^2, the slope (the derivative dD/dL^2) of the resulting curve yields the induced drag factor:

$$k = dD/dL^2 \pi q b^2. \tag{9}$$

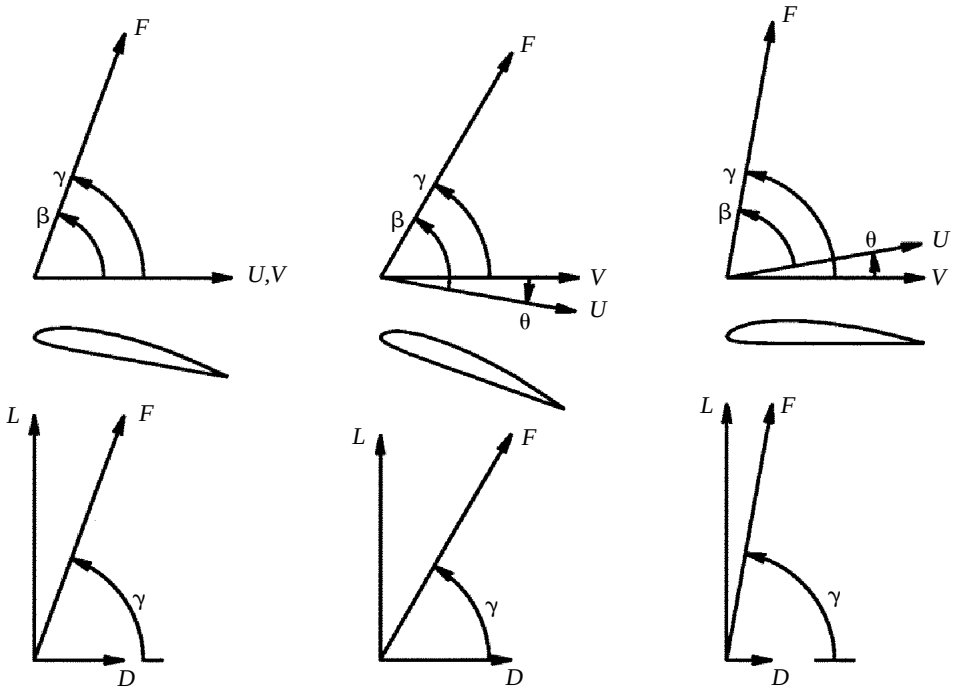

Fig. 4. Effects (left to right) of three different local air-flow velocities (U) on the lift and drag of a wing exposed to a constant, horizontal free-stream velocity V. U and V have the same magnitudes, but U is horizontal only in the left-hand diagrams. The top row of diagrams shows the angles between the aerodynamic force (F), the local flow velocity and the free-stream velocity. The angle (θ) between U and V varies from 0 in the left-hand diagram to negative (downward local flow) in the middle diagram, to positive (upward local flow) in the right-hand diagram. The angle (β) between F and U is constant, as is the magnitude of F. The angle (γ) between F and V varies. The middle row of diagrams shows the aerofoil of the wing, which rotates so that it always has the same angle of attack relative to U. The bottom row of diagrams shows the components of F: lift (L) and drag (D) are perpendicular and parallel to V by definition. The left-hand diagram with the local flow equal to V is for reference. The middle and right-hand diagrams show how downward and upward local flows increase and decrease drag, respectively. Lift changes less than drag in the diagrams.

For bird wings, the 'span factor' (M) is more convenient to use than k because it is easier to envision how natural selection might operate on wing span:

$$M = 1/k^{1/2}. \quad (10)$$

The greater the span factor, the less the induced drag for a given amount of lift. The span factor is simply the ratio of the effective wing span to the actual wing span (b). The effective wing span (b_e) combines wing span and k into a single variable:

$$b_e = b/k^{1/2}. \quad (11)$$

Experimental approach

Unfortunately, no single measurement on a living bird shows conclusively whether slotted tips act as winglets and reduce the induced drag factor. For example, one could measure drag before and after cutting off the ends of the tip feathers of a bird gliding in a wind tunnel. This operation may change the induced drag factor, but it also changes the span, area and pitching moment of the wings (Tucker, 1992). The bird compensates by adjusting the span and angle of attack of its wings and tail. Changes in induced, profile and tail drag must all be accounted for in determining the induced drag factor.

This study investigates a more controlled apparatus: a model wing mounted on a force transducer in a wind tunnel. The model wing of necessity had a different shape from an actual bird wing, because the wing tip and base wing of the model were separate parts. I could control the angles of attack of both parts independently and measure aerodynamic forces on them. I used different tips with the base wing, including one made from tip feathers from a Harris' hawk (*Parabuteo unicinctus*). In addition, I used a flow visualization technique to investigate whether winglets spread the vortex sheet vertically in their wake.

Experiments with the model wing answered three questions.

(1) Does the base wing generate upwash at the wing tip that reduces the drag of the tip, as described by Spillman (1987)? These experiments used a yawmeter to measure the direction of air flow at the end of the base wing. They also measured how much the aerodynamic force on the wing tip rotated forward as the upwash at the end of the base wing tilted progressively upward with increasing base wing lift.

(2) Does the drag reduction at the tip in question 1 influence the drag of the base wing? These experiments measured the drag on the base wing at a fixed angle of attack while the angle of attack of the wing tip varied.

(3) What is the effective wing span of a wing with a slotted tip? These experiments measured the lift and drag of a combined base wing and wing tip at different angles of attack, and used the partition model to find span factors.

Materials and methods

Materials

Wind tunnel

The wind tunnel (described in detail in Tucker and Parrott, 1970; Tucker and Heine, 1990) had a closed, rectangular working section with a cross-sectional area of 1.5 m^2. All

measurements were made at a constant air speed of $12.6\,m\,s^{-1}$. This speed was calculated from measurements of dynamic pressure (q), using an air density of $1.23\,kg\,m^{-3}$, the density of air at sea level in the US Standard Atmosphere (von Mises, 1959).

Yawmeter

The yawmeter measured the direction of the air velocity vector projected onto the vertical *x*,*z* plane. The yawmeter probe (Fig. 5) was similar to the one illustrated in Fig. 4.48a of Gorlin and Slezinger (1966) and consisted of two stainless-steel tubes soldered together along their long axes. The tubes were 91mm long and had outside and inside diameters of 1.27 and 0.79mm, respectively. One end of the probe had a wedge-shaped tip with an included angle of 90°. The other end connected with flexible plastic tubing to a differential electronic manometer (Datametrics Barocel 1174). I aligned the long axis of the probe with the air flow by rotating the probe 180° around its long axis. The yawmeter could measure the direction of air flow to within 0.25°.

A remote-controlled device in the wind tunnel held the probe at the end of a shaft 230mm long and 4.8mm in diameter. The device could point the probe in any direction in the *x*,*z* plane without changing the position of the probe's tip.

Force transducer

The force transducer was a strain gauge device (described in Tucker, 1990) that responded to force components in a plane. It measured either direction (within 0.25°) or magnitude, depending on its orientation to the force component. The transducer had two orthogonal axes: a null axis and a sensitive axis. A force applied parallel to the null axis caused no change in the voltage output, but a force in any other direction in the plane had a component that was parallel to the sensitive axis. This component caused a change in

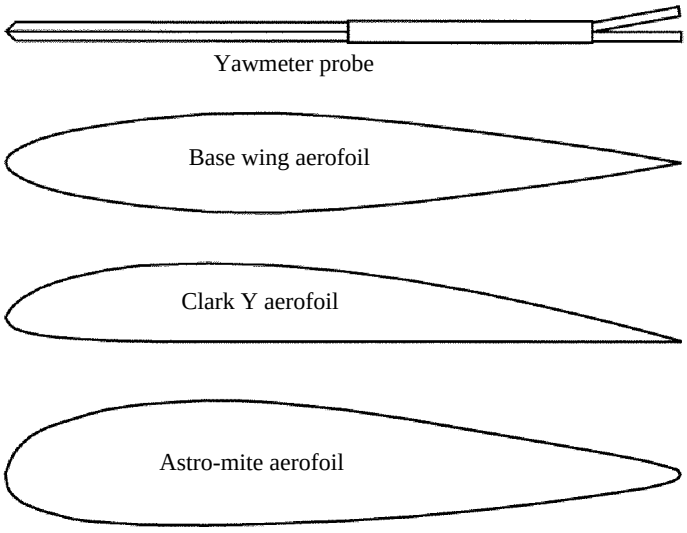

Fig. 5. The yawmeter probe and the aerofoils of three wings used in this study. See text for dimensions.

voltage output that was proportional to the magnitude of the component. I calibrated the transducer for both direction and magnitude with weights attached to a thread that ran over a pulley with negligible starting torque.

Wing balance

This device (Figs 6 and 7) measured the direction of a force or the magnitude of a force component on either the base wing or the wing tip. It consisted of a mounting plate, the transducer attached to the mounting plate and a streamlined shroud that covered the transducer and mounting plate. The transducer could be rotated on the mounting plate to change the direction of the null axis. A vertical steel rod extended from the floor of the building through the floor of the wind tunnel and supported the wing balance, isolating it from the mechanical vibration of the tunnel.

Either the base wing or the wing tip of the model wing could be attached to the transducer. The other part was attached to the mounting plate, and neither part touched the other. The angles of attack of both parts could be adjusted independently.

Base wing

The base wing (made from aluminium sheet 0.5mm thick) had a semi-span of 203mm from root to end, a chord of 175mm and a thickness of 26mm. Its aerofoil (Fig. 5) was symmetrical and was calculated from the standard coordinates for a Navy number 1 strut (Tucker, 1990). Although this aerofoil did not duplicate the cambered aerofoils in a bird wing, it made the base wing thick enough to contain the shaft and mount that held the wing tip (see description of the Clark Y tip below). The end of the base wing was open to allow the wing tip to rotate and change its angle of attack. A boss (Fig. 7) at the root of the base wing was attached to either the mounting plate or the force transducer of the wing

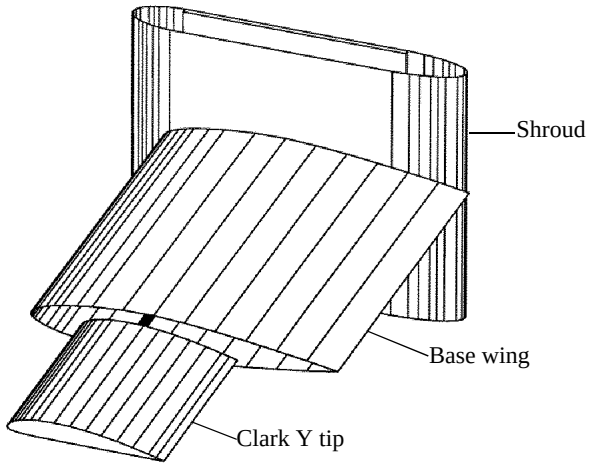

Fig. 6. The wing balance with the base wing and the Clark Y tip attached. The vertical structure is the streamlined shroud that covers the force transducer. The tip shaft can be seen between the base wing and the tip. It extends through the base wing and supports the tip. The shroud is 152mm high.

balance. The reference line of the base wing was the line of symmetry of the aerofoil, and the angle of attack of the base wing could be set by rotating the boss in its mounting.

Clark Y wing tip

This tip (Figs 6, 8) was machined from balsa wood (Tucker, 1990) and extended 113mm beyond the end of the base wing. Its chord was 89mm and its aerofoil (Fig. 5) was calculated from the standard coordinates of a Clark Y aerofoil (National Advisory Committee on Aeronautics, 1926). A tip shaft 4.8mm in diameter held the wing tip in place at the end of the base wing. The tip shaft ran from the wing tip through the boss at the root of the base wing and connected to either the mounting plate or the force transducer of the wing balance. The reference line of this tip was the straight line that forms most of the bottom of the aerofoil, and the angle of attack of the tip could be set by rotating the tip shaft in its mounting.

Feathered wing tip

This tip (Fig. 8) consisted of a feather clamp and primary wing feathers 6–9 from a Harris' hawk. Harris' hawks have 10 primary feathers on each wing, with primary 10 on the leading edge of the wing. Primaries 6–9 are the largest feathers that form the slotted tip (illustrated in Tucker, 1992) in this bird. The clamp held the shafts of the feathers at the same angles and spacing that they had in photographs of the gliding bird. The tip shaft

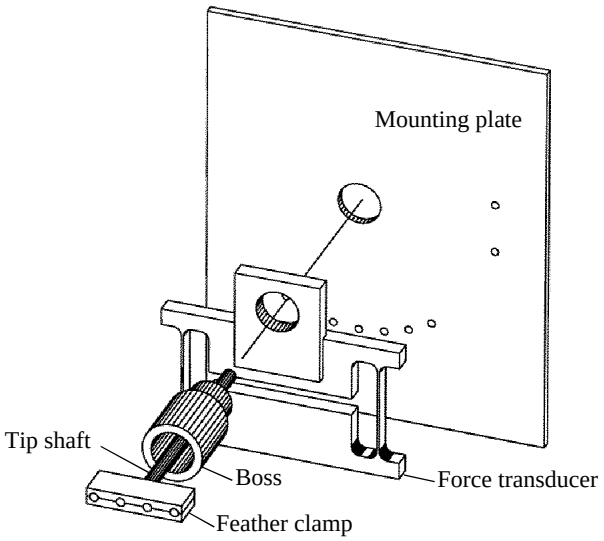

Fig. 7. An exploded, internal view of the wing balance. The tip shaft that supports the wing tip is shown with the feather clamp at its end. This clamp holds the four feathers in the feathered tip. The boss attaches to the base wing and can be connected to either the force transducer or the mounting plate. In the latter case, the force transducer mounts on the opposite side of the mounting plate from that shown, and the tip shaft runs through the mounting plate and attaches to the force transducer. The small holes in the mounting plate allow the force transducer to be attached in various positions so that it can measure either lift or drag. The force transducer can also rotate around the axis of the tip shaft. The mounting plate is 152mm high.

connected the clamp to either the force transducer or a mounting plate, as described for the Clark Y tip. The shaft held the clamp inside the base wing so that only the parts of the primaries that form the slots extended from the base wing into the air flow. The longest feather extended 100mm beyond the end of the base wing. The area of the tip was 0.00956 m^2. This value is the sum of the projected areas of the part of each feather that extended from the base wing, including overlap with adjacent feathers. The reference line for the feathered tip was one edge of the clamp.

Balsa feather wing tip

This tip (Fig. 9) consisted of three, rectangular feathers machined from balsa wood, each with a Clark Y aerofoil, a span of 115.6mm and a chord of 25.4mm. Each feather attached to a separate clamp on an aluminium plate. The clamps held the feathers at fixed dihedral and sweepback angles, but allowed their angles of attack to be adjusted (Fig. 9). I adjusted the angle of attack of each feather to maximize the L/D of the whole tip when the tip was in place at the end of the base wing.

The tip shaft connected the plate to the force transducer, as described for the Clark Y tip. The reference line for a feather was the straight line that forms most of the bottom of the aerofoil. The total projected area of all the feathers was 0.00881 m^2.

Flow visualization

I used a method for flow visualization similar to one described by Spedding (1987): a wing moved through a cloud of neutrally buoyant, helium-filled bubbles about 3mm in diameter that served as markers in the air. Two bubble generators created the bubble cloud in still air in a room. The cloud was disk-shaped, about 0.7m in diameter in the y,z plane and about 0.3m thick in the x direction. A trolley carried a wing through the cloud of bubbles at a speed of 3.8 $m\,s^{-1}$. A stationary camera photographed the bubbles in the wake of the wing tip from a point directly behind the wing tip – i.e. the camera pointed in

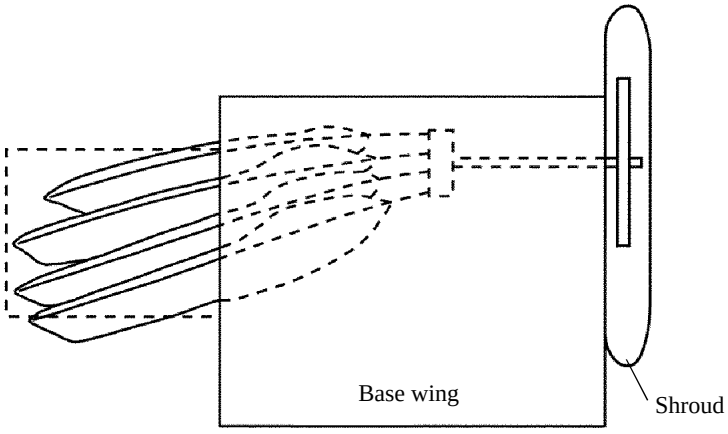

Fig. 8. A top view of the wing balance with the base wing and the feathered tip mounted on it. Dashed lines show the tip shaft, the feather clamp and the parts of the tip feathers that are inside the base wing. Dashed lines also show the outline of the Clark Y tip.

the direction of wing movement and its optical axis was parallel to the *x* axis. A computer opened the shutter of the camera after the wing had passed through the bubble cloud and moved one wing span beyond it. The computer then fired four electronic flash units at 7.83ms intervals and closed the camera shutter. The four images of each bubble in the photograph showed the bubble's trajectory projected onto the *y*,*z* plane.

The wing was from a model aircraft (Astro-mite, Tucker and Parrott, 1970), had a span of 1.1m and was untwisted with a constant aerofoil (Fig. 5). The wing was slightly tapered, with a chord of 162mm at the root and 146mm at the tip. Two winglets (Fig. 10) could be attached to one end of the wing, each winglet being one of the balsa feathers described in the 'Balsa feather wing tip' section. (I used balsa feathers rather than real feathers because the wing did not move fast enough to load real feathers aerodynamically and to separate them vertically). The long axis of one winglet was parallel to the *y* axis and that of the other tilted up at an angle of 31.6°. The wing and both winglets had the same angle of attack.

Methods

Upwash and the maximum L/D *of the wing tip*

The yawmeter measured the direction of air flow at 147 points in space at the end of a base wing mounted on the wing balance. This base wing was smaller than the base wing used with different tips, but it had the same aerofoil and relative thickness. Its span and chord were 124 and 109mm, respectively. Its angle of attack was 10.5°.

For measurements of the *L*/*D* of the wing tip, the base wing attached to the mounting plate of the wing balance and the wing tip attached to the force transducer. I varied the

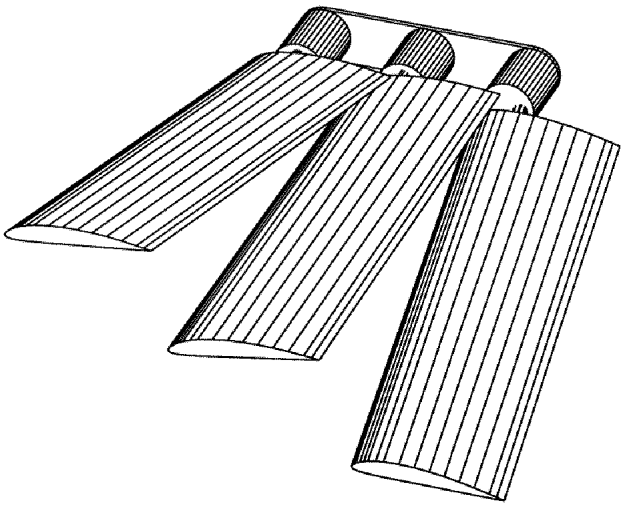

Fig. 9. The balsa feather tip. The plate with the cylindrical clamps attaches to the tip shaft inside the base wing. The following angles give the angle of attack, dihedral and sweepback, respectively, of the balsa feathers: anterior feather: 0°, 14°, 0°; middle feather: −0.25°, 7°, 5°; posterior feather: 12.5°, 0°, 10°.

angle of attack of the base wing over a range of values and, at each angle, measured the direction of the aerodynamic force on the wing tip. Then I adjusted the angle of attack of the wing tip to rotate the direction of the force as far forward as possible – i.e. to maximize the angle γ (and L/D, equation 3).

Effect of the tip angle of attack on the drag of the base wing

The base wing attached to the force transducer of the wing balance, and the wing tip attached to the mounting plate. The base wing had a constant angle of attack (13˚), but the angle of attack of the tip varied.

Lift and drag of the combined base wing and tip

These experiments measured the lift and drag of the base wing with the wing tip rigidly attached to it – i.e. the angle between the reference lines for the tip and the base wing remained constant. The combined base wing and tip attached to the transducer of the wing balance, and the angle of attack of the base wing varied.

Each wing tip had an angle of attack that approximately maximized the lift to drag ratio of the tip when the base wing had an angle of attack near 11˚. The angle of attack of the Clark Y tip was 5˚ less than that of the base wing. I set the angle of attack of the feathered tip by observing the feathers in the air flow. The feathers began bending upwards when the base wing had an angle of attack of 8˚ and reached the position for maximum L/D when the angle of attack of the base wing was 10–12˚.

I measured lift and drag for the combined wing at different angles of attack of the base wing and fitted least-squares curves to the data. During lift and drag measurements, the null axis of the force transducer was parallel and perpendicular, respectively, to the air flow within 0.25˚. I calculated curves for the span factor at different angles of attack

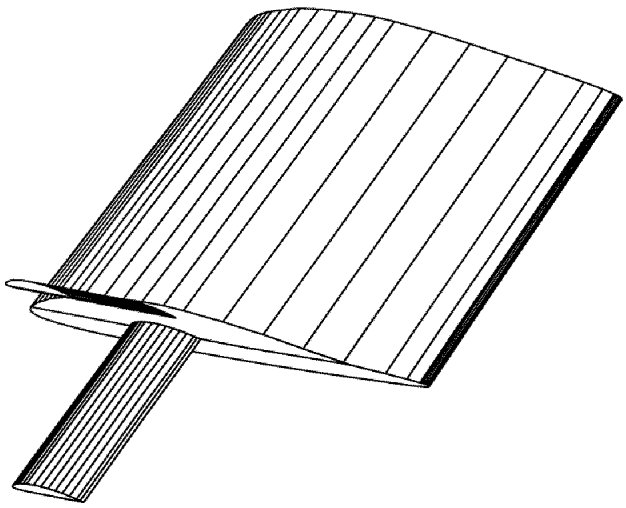

Fig. 10. The end of the Astro-mite wing used in the flow visualization experiments, with two winglets attached.

using equations 9 and 10. The derivative dD/dL^2 in equation 9 came from the fitted curves for lift and drag.

The shape of the span factor curve for a particular base wing/wing tip combination has a statistical distribution because of variation in the measured data. I investigated this distribution by using a Monte Carlo simulation (Hammersley and Handscomb, 1964).

For a particular combination of base wing and wing tip, a computer program chose a random value for angle of attack from an appropriate range and calculated the mean value of drag for this angle from the equation of the fitted curve for drag. The program then chose a random value for drag from a normal distribution with a mean equal to the mean value of drag and the same standard deviation as that of the original data around the fitted curve. Twenty-five repetitions of this Monte Carlo simulation generated a set of data that itself was fitted with a least-squares curve. The program repeated the entire procedure to fit five such curves to the drag data. The equations for these curves varied because of the variation of the drag measurements around the original fitted curve. The program used a similar procedure to generate five curves for lift at different angles of attack.

The program then used five randomly selected pairs of curves for lift and drag to obtain the derivatives dD/dL^2 and the span factor at different angles of attack for each combination of base wing and tip. The resulting plots of span factor *versus* angle of attack show the variation that can be expected in a curve because of variations in the original lift and drag measurements.

Flow visualization

The photographs showed the bubble trajectories in the wake of the wing under two conditions: when the wing had no winglets and when it had two winglets attached to one end. I enlarged the negatives to 0.55 times life size and digitized points on the bubble trajectories to within 0.25mm. The optics of the camera–enlarger combination introduced no measurable distortion into the enlargements (Tucker and Heine, 1990). A line between the two end bubbles described a straight trajectory. I described curved trajectories by digitizing a third point between the end bubbles and fitting a circle segment through the three points.

Results

Upwash and the maximum L/D *of the wing tip*

Air flowed upwards in most of a region at the end of the base wing (Fig. 11). The angle of attack of the base wing had a dramatic effect on the maximum *L/D* of the feathered tip: the maximum *L/D* more thandoubled as the angle of attack of the base wing increased from 2 to 14˚ (Fig. 12 and Table 1). In contrast, the *L/D* of the Clark Y tip was relatively independent of the angle of attack of the base wing, and that of the balsa feather tip was intermediate.

Effect of tip angle of attack on the drag of the base wing

The angle of attack of the Clark Y tip had a dramatic effect on the drag of the base wing when the base wing had a fixed angle of attack of 13˚ (Fig. 13 and Table 1). As the angle of attack of the tip increased, so did the drag of the base wing.

Yawmeter measurements showed that downwash 25mm beneath the base wing increased as the angle of attack of the Clark Y tip increased. At the end of the base wing, the downwash angle (measured between the *x* axis and the direction of the local velocity projected on the *x,z* plane) increased by 1.75˚ as the angle of attack of the Clark Y tip

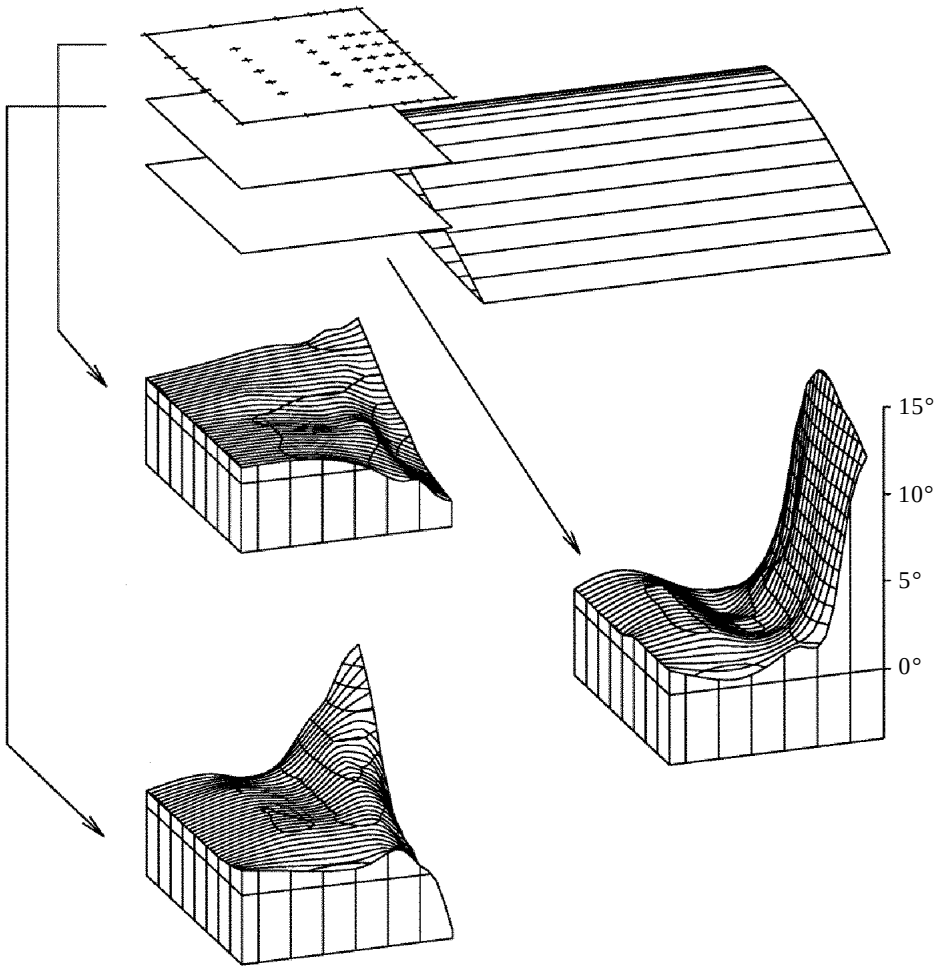

Fig. 11. Contour maps of the vertical air flow directions at points in three horizontal planes at the end of the base wing. Each map shows the vertical angles from the *x* axis of the local air velocity vectors projected on the vertical *x,z* plane. Arrows connect the horizontal planes with the corresponding contour maps, and the right-hand map shows the angular scale (in degrees). The contour interval is 1˚, and the distance between the vertical lines along the base of each map represents 10mm. The figure is a scale drawing of the maps, the base wing and the three horizontal planes. The crosses on the top-most plane mark points where flow direction was measured. The measurement points on the other planes are in register below the crosses. The right-hand edges of the horizontal planes are in the vertical plane that contains the aerofoil at the end of the wing. The map for the bottom horizontal plane does not extend to the right-hand edge because most of the points along that edge were within the aerofoil at the end of the wing.

increased from 0 to 12°. At a point 75mm from the end of the base wing towards the root, the downwash angle increased by 0.75° under the same conditions.

The angle of attack of the feathered tip had the opposite effect on the drag of the base wing under the same conditions (Fig. 13 and Table 1). As the angle of attack of the tip increased, the drag of the base wing decreased slightly. The tip produced lift at all angles of attack greater than −2° and reached maximum *L/D* at an angle of attack of 5.5°,

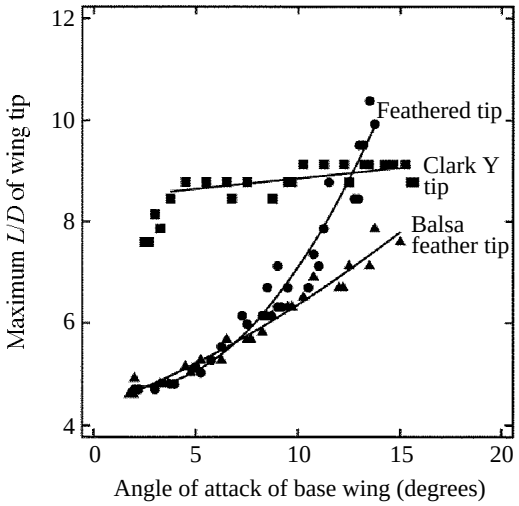

Fig. 12. The effect of the angle of attack of the base wing on the maximum lift to drag ratios (*L*/*D*) of three tips: the Clark Y tip (squares), the feathered tip (circles) and the balsa feather tip (triangles).

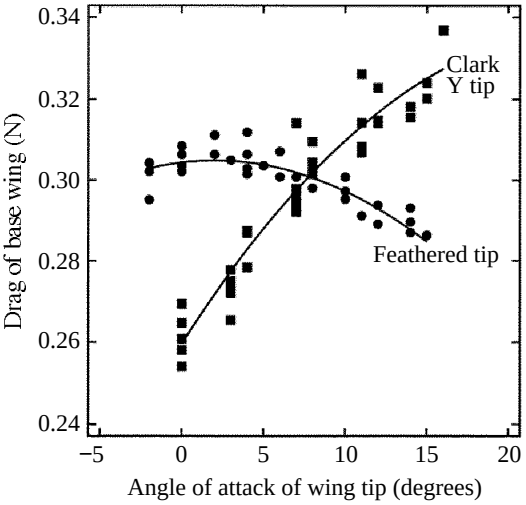

Fig. 13. The effect of the angle of attack of the wing tip on the drag of the base wing for two tips: the Clark Y tip (squares) and the feathered tip (circles). The angle of attack of the base wing was fixed at 13°. The positions of the feathers in the feathered tip indicated that the *L/D* of the tip was 0 at an angle of attack of −2° and 9.2 at an angle of attack of 5.5°.

judging from the position of the feathers. The downwash angles at the points beneath the base wing described in the previous paragraph increased by less than 0.25° as the angle of attack of the tip increased.

Lift and drag of the combined base wing and wing tip

The lift and drag of the combined base wing and wing tip varied with angle of attack for both the Clark Y tip and the feathered tip (Figs 14, 15 and Table 1). As a reasonable approximation, lift varied linearly and drag varied parabolically over a wide range of angles of attack, as is typical of conventional wings.

The span factor (*M*) of the wing with the Clark Y tip decreased as the angle of attack increased, but that of the wing with the feathered tip remained constant (Fig. 16).

Flow visualization

The flow patterns in the wake of the wing tip differed for the wing tip with and without

Table 1. *Coefficients for* L/D, *lift and drag equations*

X	*Y*	C_0	C_1	C_2	S.D.$_{Y.X}$	*N*	Equation number
Variable base wing angle of attack							
Base wing	Maximum wing tip *L/D*						
2.0–13.8	Feather tip	4.94	−0.168	0.0384	0.360	30	15
3.8–15.5	Clark Y tip	8.43	0.042	0	0.194	21	16
1.8–15.0	BF tip	4.34	0.146	0.0056	0.176	25	17
Variable tip angle of attack, base wing angle of attack fixed at 13°							
Tip	Base wing drag (N)						
−2.0 to +15.0	Feather tip	0.304	0.0006	−0.000120	0.0033	36	18
0.0–16.0	Clark Y tip	0.260	0.0063	−0.000130	0.0064	33	19
Combined base wing and feathered tip							
Base wing							
2.1–14.7	Lift (N)	−0.130	0.1785	0	0.0516	29	20
6.2–17.0	Drag (N)	0.147	−0.0023	0.00144	0.0051	22	21
Combined base wing and Clark Y tip							
Base wing							
3.2–17.3	Lift (N)	−0.265	0.2459	−0.00324	0.0387	23	22
5.2–18.0	Drag (N)	0.125	−0.0067	0.00187	0.0054	21	23

Equations are descriptive, of the form $Y=C_0+C_1X+C_2X^2$ and fitted by least-squares regression.

X is an angle of attack, in degrees. The column entries under *X* indicate the structure that the angle of attack describes, and the range of the angle of attack.

The column entries under *Y* indicate the quantity that *Y* represents and the type of wing tip, where applicable.

S.D.$_{Y.X}$ is the standard deviation of *Y* around the fitted curve, and *N* is the sample size.

BF tip, balsa feather tip.

winglets (Figs 17, 18). Without winglets, the vortex in the wake of the wing circulated around a vortex filament (von Mises, 1959) that appears in cross section as a point in the *y*,*z* plane. With winglets, the vortex spread both horizontally and vertically and circulated around a cylindrical vortex sheet (von Mises, 1959) with a core that appears in cross section as a circle in the *y*,*z* plane. The air within the circle had virtually no circulation.

Blick *et al.* (1975) measured vorticity close behind (1.7 wing chord lengths) a wing tip with separated feathers and found individual vortices behind the feathers.

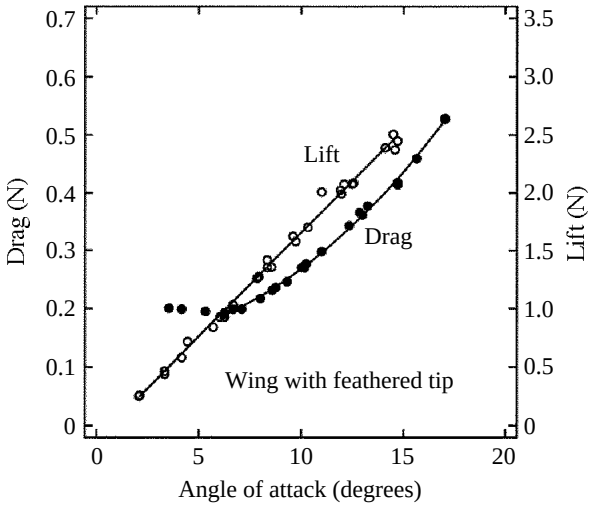

Fig. 14. The lift (open circles) and drag (filled circles) of the base wing combined with the feathered tip at different base wing angles of attack.

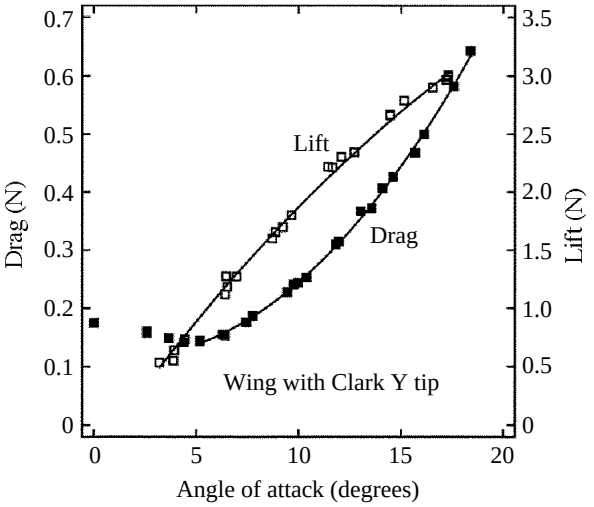

Fig. 15. The lift (open squares) and drag (filled squares) of the base wing combined with the Clark Y tip at different base wing angles of attack.

Discussion

Upwash and the maximum L/D *of the tip (base wing effect)*

Upwash at the end of the base wing increases the *L/D* of the wing tip (Fig. 12). The slope of the curve that relates the *L/D* of the wing tip to the angle of attack of the base

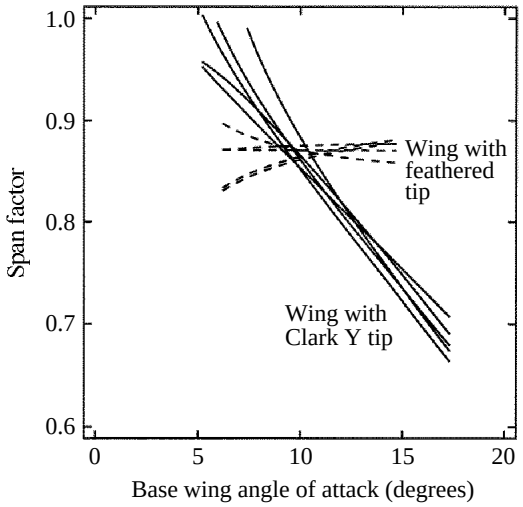

Fig. 16. Span factors for the base wing combined with two different tips at different base wing angles of attack. The five solid lines, which show the variation in the span factor of the wing with the Clark Y tip, were calculated from a Monte Carlo simulation (see text). Likewise, the five dashed lines describe the wing with the feathered tip.

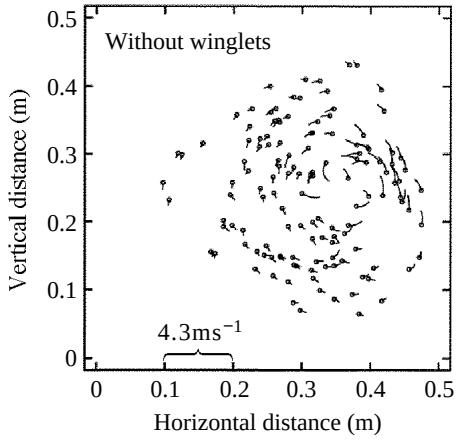

Fig. 17. Helium bubble trajectories in the wake of the Astro-mite wing tip without winglets. Each trajectory is the projection on the *y,z* plane of a bubble's path through space in 23.5ms. The trajectories end at the ends of the lines marked with circles and circulate about a point in the *y,z* plane. The axes indicate both distance and speed: a trajectory that is 0.1m long moves at 4.3 ms^{-1}. This figure superimposes trajectories from several photographs each of which showed the same view of the wing's path through space.

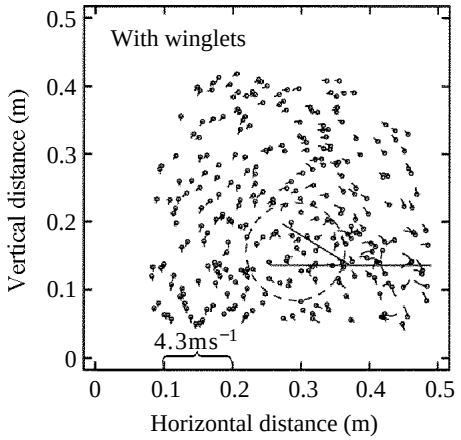

Fig. 18. Helium bubble trajectories in the wake of the Astro-mite wing tip with two winglets. Conventions are the same as in Fig. 17. The trajectories circulate around a non-circulating region of bubbles, enclosed within a dashed circle. The circle cuts solid lines that represent the trailing edges of the winglets and the end of the base wing. The trailing edges show the scale of the wing tip but not its position in space: both it and the bubbles have moved since it passed through the bubbles.

Table 2. *Forces and force coefficients for wing tips, base wing and combined base wing and tip*

	Tip		Base wing		Total	
	Force	Coefficient	Force	Coefficient	Force	Coefficient
Clark Y tip						
Angle of attack	9°		13°			
Drag	0.048	0.056	0.306	0.088	0.354	0.082
Lift	0.43	0.50	1.95	0.56	2.38	0.55
Feathered tip						
Angle of attack	5.5°		13°			
Drag	0.057	0.061	0.303	0.088	0.360	0.082
Lift	0.53	0.56	1.67	0.48	2.20	0.50

The angles of attack are coincident angles, defined in the text.

Forces are given in newtons, and the coefficients are dimensionless lift (C_L) or drag (C_D) coefficients: $C_L=L/(qS)$, $C_D=D/(qS)$; where S is the projected area of the tip, base wing or the total of both.

The drag of the wing with the feathered tip was partitioned as follows (A_{bw} = the coincident base wing angle of attack, and A_t = the coincident tip angle of attack. Equations 15–23 from Table 1): equation 21, evaluated at A_{bw}, gives the total drag of the combined base wing and tip. Equation 18, evaluated at A_t, gives the drag of the base wing alone. The difference between these two drags is the tip drag. (Equations 23 and 19 similarly partition the drag of the wing with the Clark Y tip.)

The lift of the wing with the feathered tip was partitioned as follows: equation 15, evaluated at A_{bw}, gives the L/D of the tip. This value, multiplied by the drag calculated in the previous paragraph, gives the drag of the tip. Equation 20, evaluated at A_{bw}, gives the total lift of the combined base wing and tip. The difference between these two lifts is the lift of the base wing. (Equations 16 and 22 similarly partition the lift of the wing with the Clark Y tip.)

wing measures this 'base wing effect'. The base wing effect was much larger for the feathered tip than for the Clark Y tip. When the base wing had an angle of attack of 12°, the base wing effect on the feathered tip was 18 times that on the Clark Y tip: 0.754 per degree *versus* 0.042 per degree. The base wing effect on the balsa feather tip shows that artificial feathers also respond to upwash.

Most of the change in L/D with the base wing effect results from a change in drag rather than lift (Fig. 4). The ratio between the change in drag and the change in lift can be computed as follows. When the direction of aerodynamic force (F) on the tip tilts from γ_1 to γ_2, the change in drag (ΔD) is:

$$\Delta D = F(\cos\gamma_2 - \cos\gamma_1). \tag{12}$$

The corresponding change in lift is:

$$\Delta L = F(\sin\gamma_2 - \sin\gamma_1). \tag{13}$$

If $\gamma_2 - \gamma_1$ is small, $\Delta D/\Delta L$ approximates the derivative dD/dL and $-L/D$, since:

$$dD/dL = d\cos\gamma/d\sin\gamma = -\tan\gamma = -L/D. \tag{14}$$

The changes in tip drag from the upwash at the end of the base wing are at least five times the changes in tip lift, judging from the values of L/D in Fig. 12.

Partitioning of lift and drag between base wing and wing tip

Three variables influence the lift and drag force components on the base wing and tip: the type of tip (feathered or Clark Y), the angle of attack of the base wing and the angle of attack of the tip. These angles varied over certain ranges in different experiments with both tip types, as summarized by the equations in Table 1. At particular tip and base wing angles of attack, the solutions of these equations coincide and describe the aerodynamic force on a combined base wing and wing tip. Table 2 shows these 'coincident angles' for each tip type. Table 2 also shows lift and drag of the combined wing, partitioned into the lift and drag on the tip and on the base wing.

Reduction of drag by the feathered tip

The upwash at the end of the base wing and the resulting large base wing effect on the feathered tip reduce the drag of the entire wing. Upwash increases the L/D of the tip (Fig. 12), and the increase does not increase the drag of the base wing (Fig. 13).

The reduction in drag due to the slotted tip can be quantified by comparing the drag of the combined base wing and feathered tip (Table 2) with the drag of a combined base wing and hypothetical tip that does not exhibit a base wing effect. Let us assume that the L/D of the hypothetical tip has a constant value of 4.9, which is the L/D of the feathered tip when the base wing produces little upwash (Fig. 12). The total drag in Table 2 is 12% less than the total drag of a base wing with this hypothetical tip.

A reduction of drag by 12% is consistent with theoretical calculations of reduced drag from slotted tips on non-planar wings. Such wings can have 14% to 25% less induced drag than a planar wing with the same lift and span and an elliptical lift distribution (Cone, 1962; Hummel, 1980). The reduction in total drag for the non-planar wing would

be about half this percentage, since induced and profile drag are equal for a wing at maximum *L*/*D*.

Lift and drag of the feathered tip compared to the Harris' hawk wing tip

The data in Table 2 can be used to estimate the proportion of a Harris' hawk's weight that the tips of the primary feathers support in gliding flight. When the hawk glides freely in a wind tunnel at maximum *L*/*D*, the lift coefficient of its wings is 0.6 (Tucker and Heine, 1990), which is the same as the lift coefficient for the feathered tip (Table 2). The feather tips, therefore, support about 10% of the hawk's weight with the wings at full span, since the tips make up about 10% of the full-span wing area (calculated from data in Tucker, 1992). The drag coefficient of the feathered tip is somewhat more than that of Harris' hawk wings: 0.06 from Table 2 *versus* 0.04 for the hawk gliding at maximum *L/D* in a wind tunnel (computed from Tucker and Heine, 1990). Not much significance can be attached to this difference, because the model base wing could have a different base wing effect from the actual base wing.

Span factors of the combined base wing and wing tip

The span factors are markedly different for the base wing with the feathered tip and with the Clark Y tip. The span factor for the base wing with the feathered tip does not change with angle of attack, but that for the base wing with the Clark Y tip declines (Fig. 16). This difference is not due to statistical variations in the measured lift and drag data, because it is larger than the range of curve shapes generated by Monte Carlo simulation.

The effect of the wing tip on the relationship between span factor and angle of attack can be explained in terms of the lift distribution along the span (see Theory). The base wing combined with the Clark Y tip is a planar wing and, theoretically, the span factor of a planar wing declines as the lift distribution departs more and more from elliptical. Evidently, the lift distribution of the combined base wing and Clark Y tip departed from elliptical as the angle of attack of the wing increased.

In contrast, the combined base wing and feathered tip changes from a planar wing to a non-planar wing as the angle of attack increases. The wing is planar at angles of attack below 8°, because aerodynamic forces are too low to bend the feathers upwards. The wing becomes non-planar at higher angles of attack as the tip feathers bend upwards. At angles of attack of above 10°, the tip feathers form slots with a configuration typical of the tip at its maximum *L*/*D*.

As the tip slots form, the vortex sheet in the wake of the wing spreads vertically as well as horizontally. The combination of vertical and horizontal vortex spreading keeps the span factor constant as the angle of attack increases.

Summary of the evidence for drag reduction

The theory and experimental results in this paper indicate from five independent points of view that the slotted tips of bird wings reduce drag in the sense that they increase the span factor.

1. Wing theory explains how the feathers in the slotted tips could reduce drag by acting as winglets, and measurements show that winglets on aircraft do reduce drag.

2. Slotted tips have reduced drag because the tip feathers are exposed to upwash at the end of the base wing. The reduction in tip drag does not increase the drag of the base wing.

3. The slotted tip maintains the span factor of the wing as the angle of attack of the base wing increases. In contrast, the span factor of the base wing with the Clark Y tip declines as the angle of attack increases.

4. In wing theory, winglets reduce induced drag by spreading vortices. Flow visualization shows that winglets on a model wing spread vorticity both horizontally and vertically.

5. Slotted tips occur in soaring birds of several families and always have vertical separation between the tip feathers in flight. The fact that vertical separation is necessary for drag reduction suggests that slotted tips result from natural selection for wing configurations with low drag.

Evolution of slotted tips

In comparison with birds that soar over land, birds that soar over the sea – for example, gulls and albatrosses – usually have longer, narrower wings with pointed tips. The reduced drag of slotted tips suggests why this difference has evolved. Slotted tips allow short wings to have the same induced drag as longer wings without tip slots – that is, to have higher span factors. Slotted tips probably increase the profile drag coefficient of the wings (Table 2; Hummel, 1980), but profile drag of gliding birds becomes small at low speeds where induced drag is high (for example, see Tucker, 1987).

Short wings can be made lighter than long wings that produce the same amount of lift because short wings have lower root bending moments (Heyson *et al.* 1977). Short wings are also more manoeuvrable: they can roll and yaw at higher angular velocities for a given tip speed.

Land and sea environments differ in that the land surface has more irregular relief and surface temperatures that vary more in time and space. As a result, winds over land, including thermals, are less predictable than those over the sea. Land birds take off by flapping in the absence of wind, manoeuvre in a spatially restricted environment and soar in unpredictable winds and while circling slowly in small thermals (Pennycuick, 1989). Short wings have advantages for these activities.

Sea birds would derive less advantage from short wings, because they probably manoeuvre less than land birds. In addition, sea birds probably fly at higher average air speeds than land birds. As air speed increases, induced drag decreases and profile drag increases. Slotted tips may become a liability at high speeds, where they could increase profile drag more than they reduce induced drag.

List of symbols

A_{bw}	coincident base wing angle of attack
A_t	coincident tip angle of attack
b	wing span
b_e	effective wing span

C_D	drag coefficient
C_L	lift coefficient
D	total drag
D_i	induced drag
$D_{i,min}$	minimum induced drag
D_{pr}	profile drag
$D_{pr,0}$	constant profile drag
F	aerodynamic force
k	induced drag factor
L	lift
M	span factor
q	dynamic pressure
S	projected area of a wing or wing tip
U	local air velocity
V	free-stream air velocity
x, y, z	spatial coordinates
β	angle between aerodynamic force and local flow
γ	angle between aerodynamic force and x axis
π	circumference/diameter of a circle
ρ	density of air
θ	angle between local flow and the x axis

This study was supported by a grant (453-5905) from the Duke University Research Council; Service Order number 50181-0-0832 from Mark Fuller, US Fish and Wildlife Service to Duke University; and a grant (BSR-9107222) from the National Science Foundation.

References

ASAI, K.(1985). Theoretical considerations in the aerodynamic effectiveness of winglets. *J. Aircraft* **22**, 635–637.

BETZ, A. (1925). A method for direct determination of wing-section drag. *National Advisory Committee for Aeronautics Tech. Memo* **337**.

BLICK, E. F., WATSON, D., BELIE, G. AND CHU, H. (1975). Bird aerodynamic experiments. In *Swimming and Flying in Nature*, vol. 2 (ed. T. Y.-T. Wu, C. J. Brokaw and C. Brennan), pp. 939–952. New York: Plenum Press.

CONE, C. D., JR (1962). The theory of induced lift and minimum induced drag of non-planar lifting systems. *National Aeronautics and Space Administration, Tech. Rept* **R-139**.

CONE, C. D., JR (1964). A mathematical analysis of the dynamic soaring flight of the albatross with ecological interpretations. *Virginia Institute of Marine Science, Special Scientific Report* **50**, 1–104.

DURAND, W. F. (1943). *Aerodynamic Theory*, vol. II. Pasadena: Durand Reprinting Committee, California Institute of Technology.

FLECHNER, S. G., JACOBS, P. F. AND WHITCOMB, R. T. (1976). A high subsonic speed wind-tunnel investigation of winglets on a representative second-generation jet transport wing. *National Aeronautics and Space Administration Tech. Note* **D-8264**.

GORLIN, S. M. AND SLEZINGER, I. I. (1966). *Wind Tunnels and Their Instrumentation*. Jerusalem, Israel: Israel Program for Scientific Translations.

GRAHAM, R. R. (1932). Safety devices in wings of birds. *J. R. aeronaut. Soc.* **36**, 24–58.

HAMMERSLEY, J. M. AND HANDSCOMB, D. C. (1964). *Monte Carlo Methods*. London: Methuen and Co., Ltd.

HEYSON, H. H., RIEBE, G. D. AND FULTON, C. L. (1977). Theoretical parametric study of the relative advantages of winglets and wing-tip extensions. *National Aeronautics and Space Administration Tech. Paper* **1020**.

HUMMEL, D. (1980). The aerodynamic characteristics of slotted wing-tips in soaring birds. In *Acta XVII Congressus Internationalis Ornithologici* (ed. R. Nöhring), pp. 391–396. Berlin: Verlag der Deutschen Ornithologen-Gesellschaft.

JONES, B. (1950). *Elements of Practical Aerodynamics*. New York: Wiley and Sons.

KATZ, J. AND PLOTKIN, A.(1991). *Low-Speed Aerodynamics: From Wing Theory to Panel Methods*. New York: McGraw-Hill, Inc.

KERLINGER, P. (1989). *Flight Strategies of Migrating Hawks*. Chicago: University of Chicago Press

KUETHE, A. M. AND CHOW, C.(1986). *Foundations of Aerodynamics*. New York: John Wiley and Sons

KYLE, C. AND EGGLESTON, D. (1992). An enthusiast's guide to the technology of the America's cup. *Scient. Am.* **266** , CUP 1–CUP 13.

LAMBERT, M. (1990). *Jane's All the World's Aircraft 1990–1991*. Surrey: Jane's Information Group Ltd.

MANGLER, W. (1938). The lift distribution of wings with end plates. *National Advisory Committee for Aeronautics Tech. Memo* **856**.

MUNK, M. M. (1921). The minimum induced drag of airfoils. *National Advisory Committee for Aeronautics Tech. Rept* **121**.

NATIONAL ADVISORY COMMITTEE ON AERONAUTICS (1926). *Technical Report* **244**, 329–368. Washington: US Government Printing Office.

NEWMAN, B. G.(1958). Soaring and gliding flight of the black vulture. *J. exp. Biol.* **35**, 280–285.

NORBERG, U.(1990). *Vertebrate Flight*. Berlin: Springer Verlag.

OEHME, H. (1977). On the aerodynamics of separated primaries in the avian wing. In *Scale Effects in Animal Locomotion* (ed. T. J. Pedley), pp. 479–494. London: Academic Press.

PENNYCUICK, C. J.(1989). *Bird Flight Performance*. Oxford: Oxford University Press.

PENNYCUICK, C. J., HEINE, C. E., KIRKPATRICK, S. J. AND FULLER, M. R. (1992). The profile drag of a hawk's wing measured by wake sampling in a wind tunnel. *J. exp. Biol.* **165**, 1–19.

SPEDDING, G. R. (1987). The wake of a kestrel (*Falco tinnunculus*) in gliding flight. *J. exp. Biol.* **127**, 45–57.

SPEDDING, G. R. (1992). The aerodynamics of flight. In *Mechanics of Animal Locomotion* (ed. R. McN. Alexander). Berlin: Springer-Verlag.

SPILLMAN, J. J. (1987). Wing tip sails; progress to date and future developments. *Aeronaut. J.* **91**, 445–453.

TUCKER, V. A.(1987). Gliding birds: the effect of variable wing span. *J. exp. Biol*, **133**, 33–58.

TUCKER, V. A.(1990). Measuring aerodynamic interference drag between a bird body and the mounting strut of a drag balance. *J. exp. Biol.* **154**, 439–461.

TUCKER, V. A. (1992). Pitching equilibrium, wing span and tail span in a gliding Harris' hawk, *Parabuteo unicinctus*. *J. exp. Biol.* **165**, 21–41.

TUCKER, V. A. AND HEINE, C. (1990). Aerodynamics of gliding flight in a Harris' hawk, *Parabuteo unicinctus*. *J. exp. Biol.* **149**, 469–489.

TUCKER, V. A. AND PARROTT, G. C. (1970). Aerodynamics of gliding flight in a falcon and other birds. *J. exp. Biol.* **52**, 345–367.

VON MISES, R.(1959). *Theory of Flight*. New York: Dover Publications.

WHITCOMB, R. T.(1976). A design approach and selected wind-tunnel results at high subsonic speeds for wing-tip mounted winglets. *National Aeronautics and Space Administration, Tech. Note* **D-8260**.

WITHERS, P. C. (1981). The aerodynamic performance of the wing in red-shouldered hawk *Buteo linearis* and a possible aeroelastic role of wing-tip slots. *Ibis* **123**, 239–247.